JOURNAL OF SPACECRAFT AND ROCKETS
Vol. 45, No. 3, May–June 2008

Adaptive Collocated Feedback for Noise Absorption in Payload Fairings

M. Austin Creasy* and Donald J. Leo†
Virginia Polytechnic Institute and State University, Blacksburg, Virginia 24060
and
Kevin M. Farinholt‡
NanoSonic, Inc., Blacksburg, Virginia 24060

DOI: 10.2514/1.34101

A method for adaptive collocated feedback is demonstrated for noise absorption in the interior of launch vehicle payload fairings. The control method consists of a self-tuning regulator that uses speakers as acoustic energy absorbers. Positive position feedback filters in series with high- and low-pass Butterworth filters are parameter-varying control filters used in the self-tuning regulator. The fast Fourier transform is used to obtain the collocated zero frequencies of the fairing, and an algorithm uses these frequencies to update the parameter-varying control filters. Temperature variations are used to change the interior acoustic resonances of a full-scale model of a Minotaur I payload fairing. Experimental results show that sound pressure level reductions of the interior full-scale model fairing are maintained above 3.3 dB over the 100- to 250-Hz frequency band as the interior acoustic resonances are changed by more than 5%.

Nomenclature

$\mathbf{B}$	=	location input vector
$\mathbf{C}$	=	location output vector
G	=	open-loop transfer function
g	=	gain
H	=	closed-loop transfer function
K	=	filter transfer function
p	=	pressure
s	=	Laplace variable
u	=	transfer function magnitude
V	=	voltage
ζ_{CL}	=	closed-loop damping ratio
ζ_f	=	filter damping ratio
ζ_m	=	modal damping ratio
η	=	filter coordinate
ξ	=	modal coordinate
ω	=	frequency
ω_f	=	filter frequency
ω_m	=	modal frequency
ω_p	=	pole frequency

I. Introduction

SATELLITE systems are subjected to the most strenuous loads that they will be exposed to in their lifetime during the first several minutes of launch, due to the severe vibroacoustic environment inside the launch vehicle payload fairing. The purpose of the fairing is to protect the satellite from damage during launch until deployment in space, but phenomena such as airflow along the walls of the fairing and booster [1], the rocket engines [2], rocket exhaust wave reflections from the ground [3], and shocks experienced during stage separations [1] produce an intense vibroacoustic environment inside the fairing. With launch cost estimates of $10,000 to $12,000 per pound [4], fairing designers have moved from conventional materials that limit noise transmission at low frequency to composite materials that subsequently decrease structural damping and increase noise transmission at low frequency. These low-frequency pressure waves, along with the associated interior boundary reflected waves, produce standing pressure waves within the fairing at relatively large amplitudes. These large-amplitude standing waves produce an overall sound pressure level (SPL) in excess of 120 dB and up to 140 dB [1,2,5] within the interior of a fairing.

The high SPL inside a payload fairing can sometimes cause debilitating damage to a payload before deployment into space. Figure 1 shows the acoustic levels expected to be experienced during liftoff for the Minotaur I payload fairing [6]. The frequency range of the peak acoustic loads is between 100 and 600 Hz, and the peak load is expected at 250 Hz. It has been estimated that anywhere from 40 to 60% of first-day satellite failures result from damage caused by excessive vibration and SPL experienced by the payload during launch [1,7]. These failures require satellite designers to make designs more robust, which usually adds a significant amount of weight to the design and offsets the advantages gained by using lighter-weight composite fairings. Another issue of importance in satellite design is the use of delicate components such as thin films, membranes, and optics. These components are especially susceptible to low-frequency excitation [1], and designing the components to withstand the loads experienced during liftoff may compromise their functionality after deployment in orbit.

The current method for reducing the SPL in payload fairings is to use acoustic blankets to absorb acoustic energy. Acoustic blankets work well at frequencies at which the blanket thickness exceeds the wavelength of sound [8]. Figure 1 shows the expected SPL in the Minotaur I rolling off at 17 dB per decade for the 1000- to 10,000-Hz frequency range. This roll-off is probably due to the use of acoustic blankets because the wavelength of sound is significantly smaller than the thickness of baseline acoustic blankets. Hughes et al. [9] found that blankets achieving a 3-dB SPL reduction in the 200- to 250-Hz frequency range of a fairing weighed four times more than the baseline blanket. Kidner et al. [5] suggested incorporating additional mass into the poroelastic layers of the blanket at random locations. These additional masses act as resonant systems that reduce the structural vibration of the fairing and therefore reduce the

Received 21 August 2007; revision received 7 December 2007; accepted for publication 13 January 2008.

*Graduate Research Assistant, Center for Intelligent Material Systems and Structures, Mechanical Engineering Department, 310 Durham Hall.
†Associate Director, Center for Intelligent Material Systems and Structures, Mechanical Engineering Department, 310 Durham Hall.
‡Research Engineer, 1485 South Main Street.

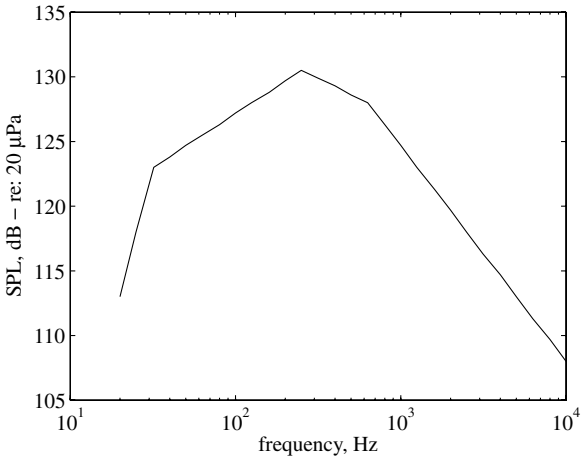

Fig. 1 Payload acoustic environment for each third-octave band expected during Minotaur I liftoff and flight with the overall sound pressure level at 140 dB.

transmission of energy into the fairing in the form of sound. The disadvantage of this approach is that it adds additional mass in the fairing, and the use of these passive devices ultimately leads to a tradeoff between the blanket thickness and the added weight and volume occupied.

The use of loud speakers to actively absorb acoustic energy from within a payload fairing or similar acoustic cavity has been researched. Lane et al. [10] reported a 6-dB peak global reduction for the first acoustic longitudinal mode in an aircraft fuselage that was 3.65 m long and 2.74 m in diameter using a 16-microphone array arbitrarily positioned throughout the fuselage. Farinholt [4] used positive position feedback (PPF) control on a fairing replica that was 2.6 m long and 0.76 m wide and reported a 4.2-dB average reduction using six microphone measurements in the 50- to 250-Hz frequency range. Kemp and Clark [1] suggested actively tuning a loud speaker in the nose of a fairing to globally absorb energy at a targeted modal frequency and reported an average 4.9-dB peak reduction at the mode located at 69 Hz (second longitudinal mode) from 16 microphone measurements within a test fairing that was 5.38 m long and 1.5 m wide at the largest diameter. Sacarcelik [11] used loud speakers in a composite test cylinder and reported a 2.2-dB global reduction in the cylinder using feedforward control and loud speakers as actuators.

The cited researchers designed the active controllers assuming a fixed enclosure without considering the fact that changes in the acoustic resonance can detune the active controller. Large temperature changes, barometric pressure changes, and different payload geometries have the potential to cause changes in the resonant frequencies of a fairing and to therefore detune an active controller. An active controller needs to be either robust enough to account for these changes and continue providing sufficient energy absorption or to be designed using some adaptation scheme to account for system changes. Research has shown that boundary changes in a finite-length duct enclosure can cause an active controller to go unstable, therefore requiring an adaptive controller [12]. The literature is abundant with information on adaptive control designs, laws, and implementation. Astrom and Wittenmark [13], Goodwin and Sin [14], Krstic et al. [15], Narendra and Annaswamy [16], and Sastry and Bodson [17] have written books explaining the basic theory of adaptive control, with introductions to the more common adaptive control schemes [gain scheduling, model referencing, and self-tuning regulators (STRs)]. Other authors explain other adaptive schemes, and numerous papers have been written about specific applications and system stability using these adaptive schemes.

For this research, we will study adaptive control in the presence of acoustic resonant frequencies that change with temperature fluctuations within a full-scale model of the Minotaur I payload fairing. A STR is used to control speakers for acoustic energy absorption as acoustic resonant frequencies shift. A comparison is made between the energy absorption capabilities of a nonadaptive controller and the STR controller as the fairing's acoustic resonant frequencies shift due to temperature variations.

II. Fairing Simulator Dimensions and Measurements

For this research, a full-scale fairing model is constructed as a test article for adaptive control. Figure 2 is a picture of the fairing simulator with a schematic of the interior components of the fairing. The fairing simulator has a 1.52-m (60-in.) diameter at the largest portion, a 0.66-m (26-in.) diameter on the end at which the control speakers are located (nose position), a 1.24-m (49-in.) diameter on the opposite end (aft position), and a total length of 5.84 m (230-in.). The 1.55-m- (61-in.)-diam Minotaur I fairing has a payload envelope with a 0.58-m (22.7-in.) nose diameter, a 1.39-m (54.7-in.) diameter at the largest portion, and a total envelope length of 3.85 m (151.5-in.) [6]. The fairing dimensions outside of the payload envelope (consisting of acoustic blankets, payload support structure, etc.) are not reported for the 1.55-m-diam Minotaur I fairing, but the simulator is assumed to provide acoustic resonant frequency values similar to the Minotaur I fairing.

A payload is placed in the simulator, as shown in the schematic (Fig. 2), with a disturbance speaker placed directly in front of the payload. Three microphones are placed in the fairing at the locations indicated in the schematic. Microphone 4 is placed between the disturbance speaker and the control speakers at an arbitrary distance. Microphones 5 and 6 are arbitrarily placed above the payload and behind the disturbance speaker, to measure the SPL reductions in the vicinity of the payload. A set of three control speakers (6 by 9 in.) located in the nose of the fairing are used for absorbing acoustic energy. For this research, the same control signal is used for each of the control speakers. Figure 3 shows the speaker array as seen from within the cavity of the fairing, with collocated microphones placed 3.8 cm (1.5 in.) from the front of each control speaker.

The system is excited with a single disturbance voltage, and the input to the system is defined as

$$\mathbf{V} = \begin{bmatrix} V_A \\ V_B \\ V_C \\ V_D \end{bmatrix} = \mathbf{B}V' \tag{1}$$

The subscripts of V refer to the speaker locations shown in Fig. 2 and 3; V' is the random disturbance voltage, with frequency content up to 1000 Hz; and $\mathbf{B}$ is a vector for which each component is either unity or zero, depending on the location of the applied input. The output of the system is the measured pressure

$$\mathbf{p} = \mathbf{C}\begin{bmatrix} p_1 \\ p_2 \\ p_3 \\ p_4 \\ p_5 \\ p_6 \end{bmatrix} \tag{2}$$

where the subscripts of p refer to the microphone locations shown in Fig. 2 and 3, and $\mathbf{C}$ is a vector or matrix that identifies which measurements are being made for a particular experiment. A matrix of transfer functions represents the input/output relationship for each of the measurement outputs over each of the actuation inputs:

$$\mathbf{p} = \begin{bmatrix} G_{1A} & G_{1B} & G_{1C} & G_{1D} \\ G_{2A} & G_{2B} & G_{2C} & G_{2D} \\ G_{3A} & G_{3B} & G_{3C} & G_{3D} \\ G_{4A} & G_{4B} & G_{4C} & G_{4D} \\ G_{5A} & G_{5B} & G_{5C} & G_{5D} \\ G_{6A} & G_{6B} & G_{6C} & G_{6D} \end{bmatrix}\mathbf{V} \tag{3}$$

where the subscripts of G refers to the microphone output and the speaker input locations, respectively; $\mathbf{C}$ is assumed to be the identity

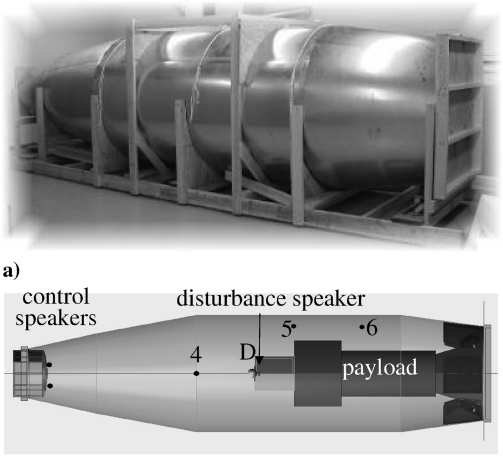

Fig. 2 Fairing simulator: a) photograph and b) interior schematic; the location of each noncollocated microphone (4, 5, and 6), the disturbance speaker (D), and the shape and proportions of the payload are shown.

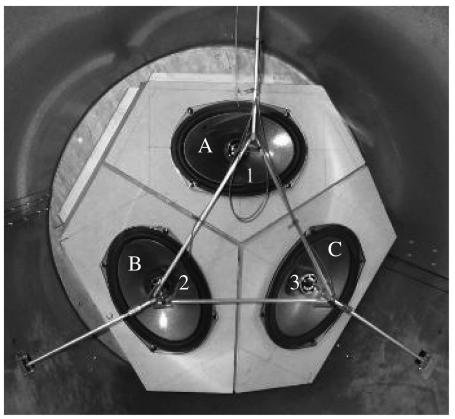

Fig. 3 Speaker orientation within the nose of the fairing; each speaker (A, B, and C) is fitted with a feedback microphone (1, 2, and 3) located 3.8 cm in front of the speaker; the same control signal is sent to all three speakers.

matrix; and **B** is a vector with each component at unity. Figure 4 shows a system diagram with the input/output relationships described in Eqs. (1–3), in which **B** and **C** can be adjusted to the particular experiment.

An average collocated transfer function G_{avg} is measured to identify the acoustic resonances of the system, where

$$\mathbf{B} = \begin{bmatrix} 1 \\ 1 \\ 1 \\ 0 \end{bmatrix} \qquad \mathbf{C} = 1/3[1 \quad 1 \quad 1 \quad 0 \quad 0 \quad 0] \tag{4}$$

Therefore, the average collocated transfer function is defined as

$$G_{\text{avg}} = \mathbf{CGB} \tag{5}$$

and produces a single transfer function. The acoustic resonant frequencies of the fairing simulator are found from the peak-magnitude responses of the transfer function G_{avg}. Figure 5 shows G_{avg} of the fairing with the internal fairing temperature at 69°F. Table 1 shows the acoustic resonant frequencies for each mode and the associated damping ratios calculated from the 3-dB down rule [18]. Each resonant frequency is related to a longitudinal mode of the simulator. The resonance of the third mode is difficult to determine because of the multiple peaks associated with that mode. These peaks are attributed to the varying diameter of the fairing and the inclusion of the payload within the fairing.

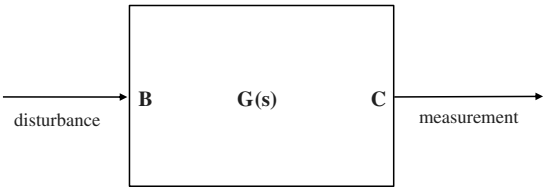

Fig. 4 Input/output relationships of the system.

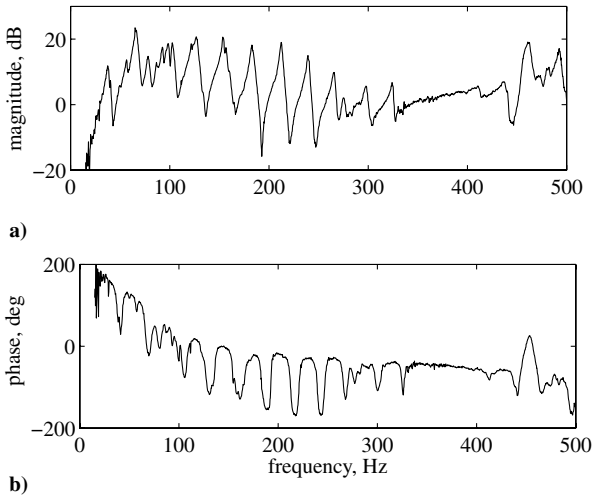

Fig. 5 Transfer function G_{avg} of the fairing.

Each mode in Fig. 5 between 20 and 250 Hz has an associated set of poles that is followed by a set of zeros. This type of pole/zero spacing should cause the phase of the transfer function to be bounded between 0 and −180 deg, but the phase has a 270-deg roll-off between 20 and 200 Hz. This roll-off is attributed to the dynamics of the measurement electronics and speaker. Above 250 Hz, the frequency between each pair of poles and the subsequent zeros is decreasing. This zero/pole proximity is seen in the phase plot of G_{avg}, starting at the mode near 265 Hz. The phase of the set of poles only drops the system phase by 90 deg before the effect of zeros increases the phase and is repeated in a similar trend for the subsequent two modes. Between 325 and 400 Hz, the magnitude and phase of the transfer function is flat due to pole/zero cancellation.

The pole/zero cancellation region is caused by the proximity of the collocated microphones to the speakers. This conclusion is determined by analyzing the matrix of transfer functions. Figure 6 shows the magnitude response of G_{1A}, G_{2A}, and G_{3A} when $\boldsymbol{B} = [1; 0; 0; 0]$. The response of G_{1A} shows a pole/zero cancellation in the 400-Hz vicinity, similar to that seen in the plot of G_{avg}. The noncollocated transfer functions do not show this trend. The same trend follows for the response of G_{2B} when $\boldsymbol{B} = [0; 1; 0; 0]$ and for G_{3C} when $\boldsymbol{B} = [0; 0; 1; 0]$ and is attributed to near-field effects of the proximity of the microphone and speaker. The pole/zero cancellation

Table 1 Frequencies and damping ratios of replica's modes

Mode	Frequency, Hz	Damping ratio
1	37.5	0.038
2	65.0	0.019
3	——	——
4	126.9	0.020
5	153.4	0.006
6	182.8	0.009
7	212.5	0.006
8	239.4	0.005
9	265.6	0.007
10	297.8	0.007
11	324.1	0.005

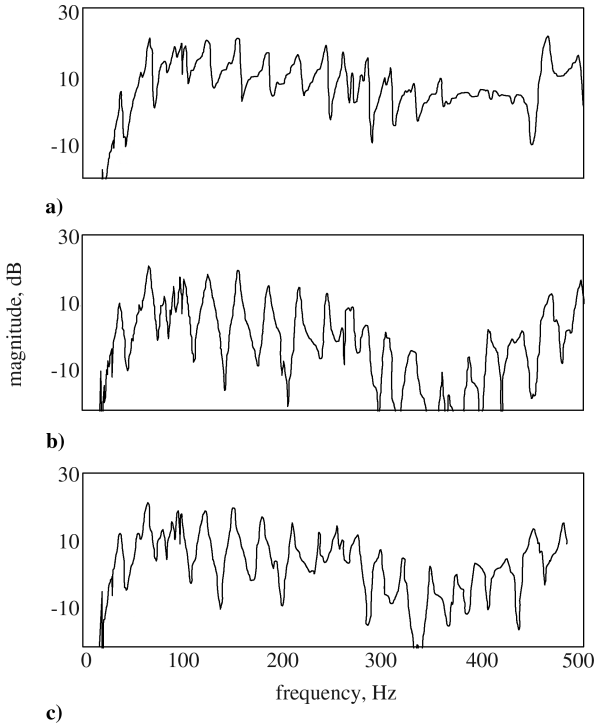

Fig. 6 Magnitudes of the transfer functions a) G_{1A}, b) G_{2A}, and c) G_{3A} with the parameter $B = [1; 0; 0; 0]$.

of G_{avg} is ideal for control because a controller can be rolled off over this frequency band. The phase and magnitude of the system are not significantly changing; therefore, as the controller dynamics change to reduce the magnitude of the controller, no system dynamics will cause potential instabilities.

III. PPF Control and Simulations

PPF control is chosen as the active control algorithm to absorb acoustic energy within the fairing. Fanson and Caughey [19] described PPF controllers using the scalar case by defining a second-order equation for the system as

$$\ddot{\xi} + 2\zeta_m \omega_m \dot{\xi} + \omega_m^2 \xi = g\omega_m^2 \eta \tag{6}$$

and a second-order equation for the filter as

$$\ddot{\eta} + 2\zeta_f \omega_f \dot{\eta} + \omega_f^2 \eta = g\omega_f^2 \xi \tag{7}$$

Therefore, a transfer function of the PPF control filter takes the form

$$K_{\text{ppf}}(s) = \frac{g\omega_f^2}{s^2 + 2\zeta_f \omega_f s + \omega_f^2} \tag{8}$$

which adds two additional poles to the system for each PPF filter used. The subscript ppf of the PPF filter is changed to the resonant frequency value for a designed PPF filter. Figure 7 shows a bode plot of a sample PPF filter normalized to the resonant frequency of the filter with unity gain. This filter design contains no zeros, which produces a flat low-frequency response for which the initial magnitude is dependent upon the filter gain, and the phase begins at 0 deg. The filter contains a set of poles that together determine the frequency of the filter resonance, cause the magnitude to roll off at 40 dB per decade after the resonant frequency, and cause a phase drop of 180 deg through the resonant frequency. The damping ratio of the filter determines the range of the phase drop and the peak-magnitude level of the filter for which a smaller damping ratio increases the peak magnitude and decreases the range of the phase drop and for which a larger damping ratio decreases the peak magnitude and increases the range of the phase drop.

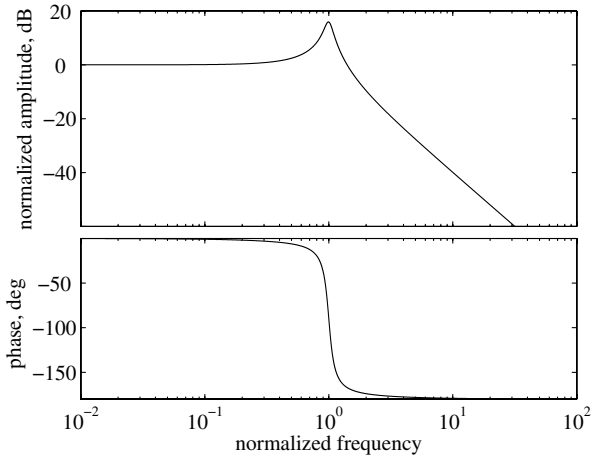

Fig. 7 Normalized bode plot of a PPF filter for which the damping ratio is set to 8%, the frequency is normalized to the resonant frequency, and the magnitude is normalized to unity.

McEver and Leo [20] derived an optimization algorithm for setting a single PPF filter for a collocated feedback controller for a system with a single set of poles followed by a single set of zeros and concluded that the algorithm could be used for multiple filters as well. The algorithm is simplified for the current research in which a positive gain is first chosen for the system. Then the ratio of the filter frequency to the pole frequency is found from

$$\frac{\omega_f}{\omega_p} = \sqrt{\frac{1}{(1 - g(\omega_p/\omega_z)^2)}} \tag{9}$$

and the ratio of the filter frequency to the pole frequency will provide the filter frequency as follows:

$$\omega_f = \omega_p(\omega_f/\omega_p) \tag{10}$$

The closed-loop damping ratio is found from

$$\zeta_{\text{CL}} = \sqrt{\frac{(\omega_f/\omega_p)^2(1-g) - 1}{4}} \tag{11}$$

and the damping ratio of the PPF filter is found from

$$\zeta_f = \frac{2\zeta_{\text{CL}}}{(\omega_f/\omega_p)} \tag{12}$$

The results from Eqs. (10) and (12) are used to find the filter transfer function from Eq. (8).

Simulations of the closed-loop system are obtained by combining the Laplace domain representation of the compensator directly with the measured transfer function. The closed-loop transfer function of a system with positive feedback [21] is

$$H(s) = \frac{G(s)}{1 - G(s)K(s)} \tag{13}$$

The closed-loop system representation is obtained by replacing the Laplace variable of Eq. (13) with frequency times the imaginary variable j:

$$H_{\text{avg}}(j\omega) = \frac{G_{\text{avg}}(j\omega)}{1 - G_{\text{avg}}(j\omega)K_{\text{ppf}}(j\omega)} \tag{14}$$

This approach allows the closed-loop transfer function of the system to be estimated using measured data without the necessity of making a system model. Here, the subscript avg of the closed-loop transfer function H indicates the collocated closed-loop measurement, similar to the open-loop measurement G_{avg}. The subscripts for the closed-loop transfer function H will follow the same nomenclature as

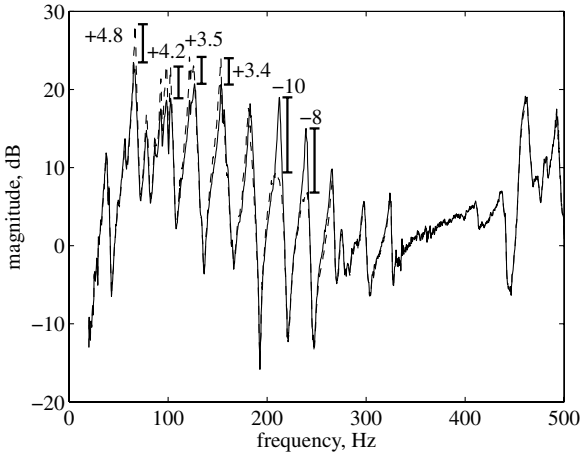

Fig. 8 H_{avg} (dashed line) overlaid on measured G_{avg} (solid line) simulating the control of two modes at 212.5 and 239.4 Hz using PPF filters for which the bars show amplifications and reductions with + and − symbols, respectively, and the associated peak dB difference of the simulation.

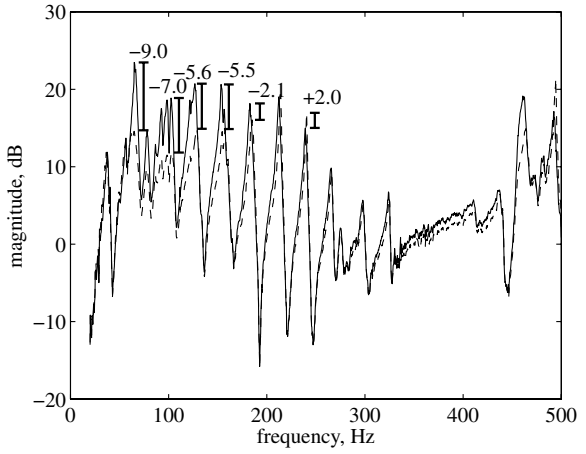

Fig. 9 H_{avg} (dashed line) with simulated proportional feedback control overlaid on measured G_{avg} (solid line) for which the bars show control reductions.

the subscripts of the open-loop transfer function G, as defined in Eq. (3).

Equations (9–12) are used to design control parameters for K_{212} and K_{239} of the fairing using the data found in Table 1 from G_{avg} and a gain of 0.02. Equation (14) is used to obtain the simulated H_{avg}, and Fig. 8 shows the plotted magnitude results of H_{avg}. The peak reductions for the resonances at 212 and 239 Hz are calculated to be 10 and 8 dB, respectively. The modes at 265 and 298 Hz show no spillover into higher modes, but the peak-magnitude responses of the resonances located at 65, the cluster between 72 and 106, 125, and 153 Hz are amplified in magnitude by 4.8, 4.2, 3.5, and 3.4 dB, respectively. This amplification is caused by the low-frequency spillover that occurs when using multiple PPF filters. Additional simulations show that this amplification of lower modes increases as additional PPF filters are included in the controller, culminating with the system going unstable.

IV. Nonadaptive Control Development

Two different methods for controlling the PPF low-frequency spillover are used in this research: proportional feedback [1,22,23] and Butterworth filters [24]. Proportional feedback is effective at reducing the magnitudes of all modes below 325 Hz, because the phase of the transfer function does not drop below −180 deg with the current pole/zero spacing. Therefore, a negative feedback loop would cause the magnitudes of the modes to be out of phase with the input and would reduce the closed-loop magnitude for those modes. Figure 9 shows the simulated results of the closed-loop system using proportional feedback for control. Magnitude reductions are evident in the second through sixth modes, which are the modes that show amplifications in the dual-mode PPF controller shown in Fig. 8. Some amplification is seen in the seventh mode (212.5 Hz) and in the mode at 492.5 Hz.

The second method uses Butterworth filters to create a bandpass filter around the mode to be controlled. This method tunes the controller to a specific frequency band and produces roll-off in the controller for all other frequencies. For this research, a sixth-order high-pass Butterworth filter is added to give the controller a 120-dB-per-decade roll-on in magnitude and a second-order low-pass Butterworth filter adds an additional 40-dB-per-decade roll-off at high frequency. An example bode plot of the high- and low-pass Butterworth filters used in conjunction with a PPF filter (shown in Fig. 10) is compared with a plot of just a PPF filter for which the filters are normalized to the PPF resonant frequency and both have unity gain. As shown in Fig. 10, the phase of the combined filter will start with an additional 540 deg and will settle 180 deg lower than with just the PPF filter. A significant low-frequency magnitude difference between the combined filter bode plot and the PPF filter

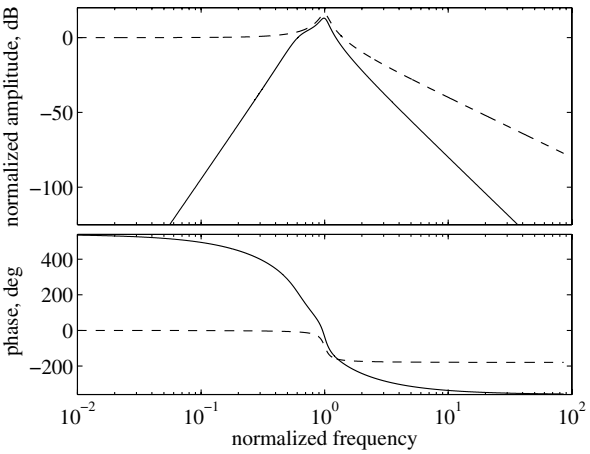

Fig. 10 Normalized bode plot of combined Butterworth and PPF filter (solid line) for which the damping ratio is set to 8%, the frequency is normalized to the resonant frequency of the PPF filter, the magnitude is normalized to unity, the cuton frequency of the high-pass filter is 40% below the PPF resonance, and the cutoff frequency of the low-pass filter is set to the PPF resonance. The bode plot of only a PPF filter (dashed line) is plotted as well for comparison.

bode plot is evident. This magnitude difference at low frequency will reduce the low-frequency spillover that occurs when only using PPF filters.

The zero frequencies preceding and following the mode to be controlled are used for the cuton (frequency at which a high-pass-filter magnitude becomes flat) and cutoff (frequency at which a low-pass-filter magnitude starts rolling off) frequencies of the Butterworth filters, respectively. Figure 11 shows the simulated closed-loop results H_{avg} with control implemented on the modes at 212 and 239 Hz. Simulations are used to optimize the PPF filter, whereby the algorithm designed for the PPF filter by McEver and Leo [20] is changed so that the damping ratio of the PPF filter is

$$\zeta_f = \frac{\zeta_{CL}}{(\omega_f/\omega_p)} \tag{15}$$

and the gain is multiplied by −1.

V. Adaptive Feedback Design

Acoustic resonant frequency changes are verified with internal temperature variations for the full-scale fairing model. Two space heaters are inserted into the system at an initial air temperature of 17.6°C (63.7°F), humidity of 32%, and a barometric pressure reading of 101.8 kPa. These measurements are made within the fairing using

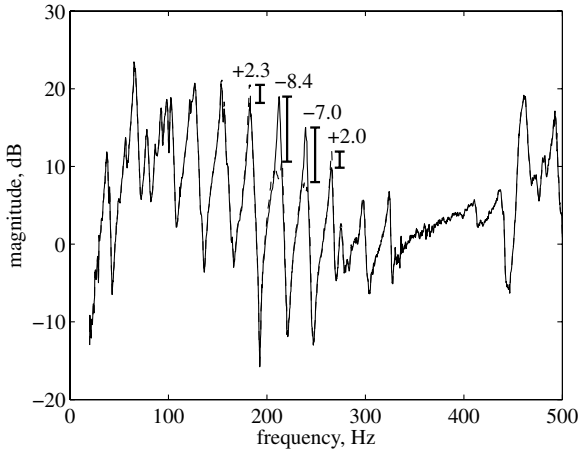

Fig. 11 H_{avg} (dashed line) overlaid on measured G_{avg} (solid line) simulating the control of two modes at 212.5 and 239.4 Hz using PPF and Butterworth filters for which the bars show amplifications and reductions with + and − symbols, respectively, and the associated peak dB difference of the simulation.

an off-the-shelf wireless weather station. G_{avg}; the average of G_{4A}, G_{4B}, and G_{4C} (defined as G_{4avg}); the average of G_{5A}, G_{5B}, and G_{5C} (defined as G_{5avg}); and the average of G_{6A}, G_{6B}, and G_{6C} (defined as G_{6avg}) are measured and the air of the internal volume is heated within the replica to 31°C (87.8°F) and the same transfer functions are remeasured. This high temperature is the maximum temperature obtainable because of internal safety devices in the space heaters. Figure 12 shows a comparison of the magnitudes of G_{avg}, G_{4avg}, G_{5avg}, and G_{6avg} at the different temperature settings. The figure shows that as the temperature is increased, the frequency of each acoustic resonance increases by 2.5 to 3.5% over the frequency range of interest for this work and that significant modal frequency variations do occur with temperature changes that could be experienced by a payload fairing.

Simulations show that peak-amplitude reductions can be affected because the shifting of mode frequencies causes filters to be detuned. Therefore, an active controller is designed to adapt to system changes. For this system, a STR is designed to accommodate to changes in the acoustic resonant frequencies. A STR consists of two feedback loops in the controller [17]. The first loop is a controller with time-varying properties and the second is a control algorithm that uses a feedback signal from the system in conjunction with a control algorithm to determine the varying properties of the controller in the first loop. The pressure measured at the collocated microphone is used as the feedback signal for both control loops.

Figure 13 shows a block diagram of the STR used in this control system. The inner-loop controller consists of time-varying PPF and Butterworth filters for which the resonance of the PPF filter and the cuton and cutoff frequencies of the Butterworth filters are the time-varying parameters. The outer loop, or algorithm loop, consists of an algorithm that designs the time-varying controller parameters from the frequency-domain response and the signal-processing capability of obtaining the frequency-domain response in real time.

The frequency-domain response is obtained by filling a buffer with a vector of measured collocated pressure p' data points. The fast Fourier transform of the vector is taken to convert the time data from the time domain to the frequency domain. Then the magnitude of the frequency-domain data is taken to obtain a vector of magnitudes with associated frequencies of the collocated position. Because the mode frequency shifts are assumed to be small with no modal overlap, the algorithm can be designed to look for maximum and minimum magnitude values over a small frequency range. The frequency values associated with the maximum and minimum magnitude values will be the frequencies of the poles and zeros of the system, respectively.

The time-varying controller consists of PPF filters combined with high- and low-pass Butterworth filters. The Butterworth filters are designed to make a bandpass filter around a particular mode using the

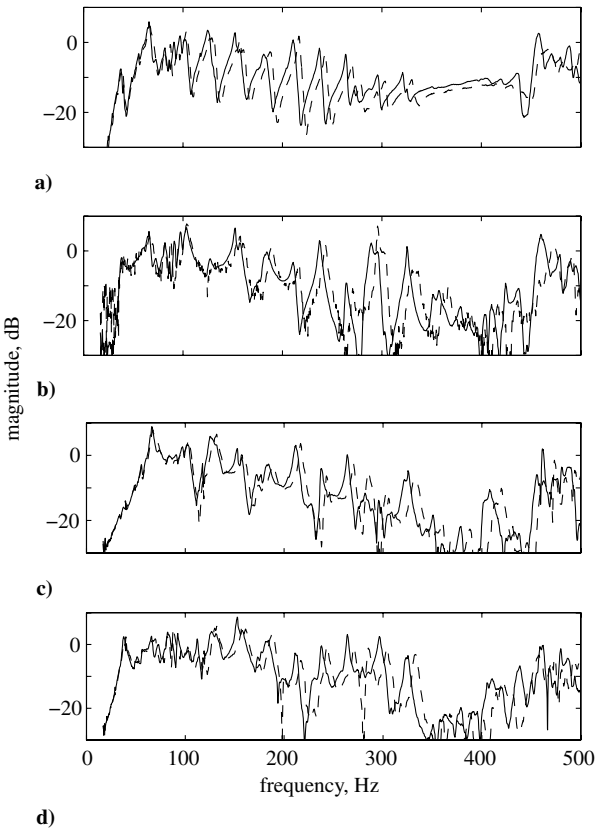

Fig. 12 Measured transfer functions a) G_{avg} b) G_{4avg}, c) G_{5avg}, and d) G_{6avg} at 31°C (dashed line) overlaid on the same measured transfer functions at 17.6°C (solid line) to show the change in the resonant frequencies at the two temperatures.

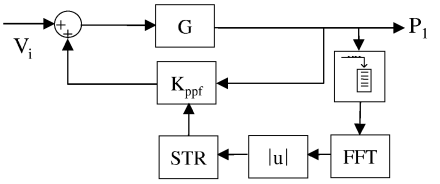

Fig. 13 Self-tuning regulator block diagram.

zero frequencies preceding and following the mode as the cuton and cutoff frequencies for the filters. The Butterworth filters are automatically adjusted as the algorithm obtains frequency values for the zeros. Only the resonant frequency of the PPF filter is time-varying. The gains and the damping ratio are maintained at values found with the control simulations using G_{avg}. The resonant frequency of the PPF filter is associated with the frequency of the zero following the mode of interest. The difference between the frequency of the zero and the value used for the PPF filter in initial control simulations is recorded in the algorithm and that difference is used as the frequencies of the zeros change. The frequencies of the zeros are chosen to vary the PPF resonances, because as damping is added to a mode, the mode may appear as a split mode and the frequency of the peak magnitude of a mode with system control may not be associated with the acoustic resonance of the system. This split-mode effect could detune the controller and could cause the SPL to increase or drive the system unstable.

VI. Experimental Results

Adaptive and nonadaptive control experiments are performed on the fairing. Simulations are used with G_{avg} when the temperature within the fairing is 18.3°C to obtain near-optimal controller

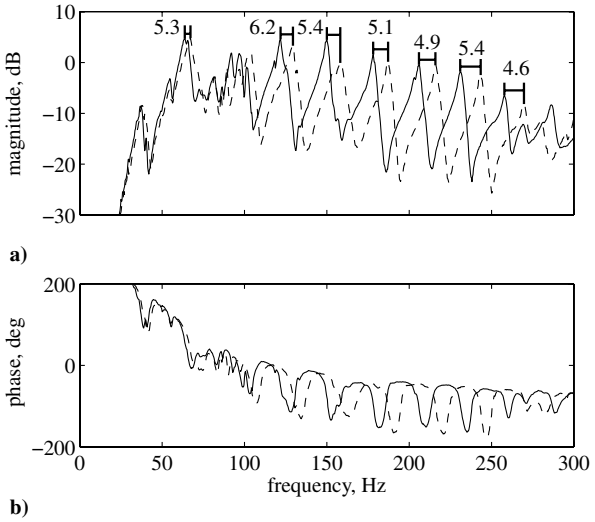

Fig. 14 Transfer functions a) magnitude and b) phase of G_{avg} (dashed line) at 31.1°C overlaid on G_{avg} (solid line) at 15.6°C with percent resonance change stated.

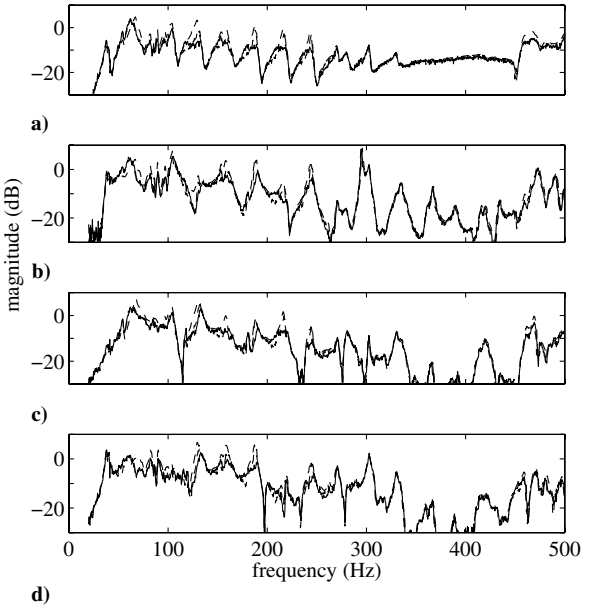

Fig. 15 Magnitudes of a) H_{avg}, b) H_{4avg}, c) H_{5avg}, and d) H_{6avg} at 31.1°C with nonadaptive controlled measurements (dashed line) and adaptive controlled measurements (solid line) overlaid on the baseline noncontrolled measurements (long dashed line) at the same temperature.

parameters for which the controller consists of negative proportional feedback, and PPF and Butterworth filters are designed for the third through eighth modes. The damping ratios for the PPF filters, all of the gains, and the filter frequency values are maintained at the values found from this simulation for the nonadaptive control experiments. For the adaptive control experiments, only the damping ratios for the PPF filters and the gains are maintained at the values found from the simulation. To obtain a larger temperature variation and therefore a larger resonant frequency change, dry ice is used to reduce the interior temperature of the fairing to 15.6°C. The use of dry ice has two effects on the interior fluid: temperature reduction and change in concentration of CO_2 in the air. This experimental setup allows a change in temperature of 15.5°C and an unknown fluid concentration change that causes an average 5.3% change in all of the acoustic resonant frequencies of interest. Figure 14 shows these two extremes for the transfer function G_{avg} for the frequency range of interest with the percent change in the acoustic resonant frequency stated.

The adaptive and nonadaptive control experiments are performed for the fairing as the acoustic resonant frequencies shift. Table 2 shows the average SPL reductions of H_{avg}, H_{4avg}, H_{5avg}, and H_{6avg} for the two temperature extremes for both experiments when control is added. Figure 15 shows the magnitude plots for each temperature extreme and measurement location compared with the baseline without control. The SPL reductions reported are for the frequency band between 100 and 250 Hz. The largest reduction is found directly in front of the control speakers, and the lowest reduction is found in the location between the disturbance speaker and the control speakers. The figure shows that there are no magnitude amplifications present in the frequencies above 300 Hz, as seen in the case when just proportional control was simulated.

Table 2 SPL reductions for temperature extremes

Temperature	Location	Adaptive	Nonadaptive
15.6°C			
	H_{avg}	4.15 dB	4.15 dB
	H_{4avg}	2.77 dB	2.77 dB
	H_{5avg}	3.89 dB	3.89 dB
	H_{6avg}	3.63 dB	3.63 dB
	Average	3.6 dB	3.6 dB
31.1°C			
	H_{avg}	3.96 dB	3.25 dB
	H_{4avg}	2.70 dB	2.07 dB
	H_{5avg}	3.32 dB	2.37 dB
	H_{6avg}	3.22 dB	2.21 dB
	Average	3.3 dB	2.5 dB

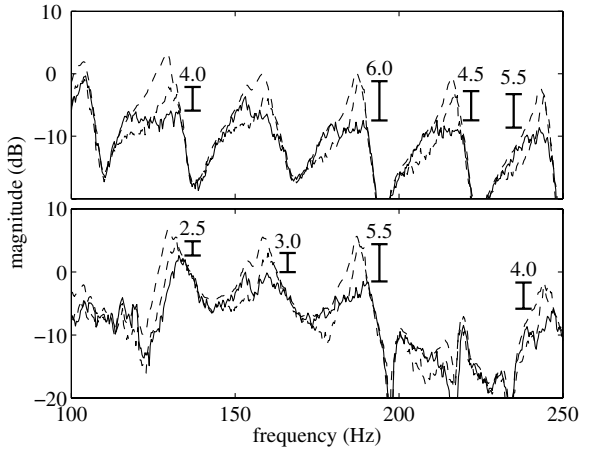

Fig. 16 Magnitudes of a) H_{avg} and b) H_{6avg} at 31.1°C with nonadaptive (tuned to control the system at 18.3°C) controlled measurements (dashed line) and adaptive controlled measurements (solid line) overlaid on the baseline noncontrolled measurement with the peak reduction difference stated between the nonadaptive and the adaptive measurements.

Figure 16 shows the magnitude of the measured transfer functions H_{avg} and H_{6avg} of the system at 31.1°C for the adaptive and nonadaptive cases compared with the baseline, for which the nonadaptive controller is tuned for the system at 15.6°C. The figure shows that the peak-magnitude responses of several of the modes are between 4 and 5 dB higher for the nonadaptive case. This reduction shows that the adaptation scheme adjusts the control parameters to account for changes in the system and maintains better overall performance for sound absorption. This adaptation scheme has several possible limitations that have not been tested in the current test configuration. Cases in which the system's resonant frequency changes cause modal frequency overlap or split modes have not been investigated with this adaptation scheme. External system disturbance has not been studied with this particular system, but was studied in a 1-D acoustic duct [12]. The results of that study indicated that the adaptation scheme worked well at reducing the internal SPL of a 1-D acoustic duct excited externally and therefore should absorb acoustic energy from within the fairing when an external disturbance is used to excite the internal acoustic modes.

VII. Conclusions

Acoustic resonant frequency changes inside a payload fairing due to temperature changes, payload size, etc., have the ability to detune an active controller used for acoustic energy absorption. This research shows that temperature variations within a full-scale model of a Minotaur I payload fairing can shift the acoustic resonant frequencies by more than 5%. A self-tuning regulator is implemented and shown to control a set of three speakers for absorbing acoustic energy from within the full-scale fairing model using proportional feedback and multiple positive position feedback filters for control. The low-frequency spillover effect that is inherent with PPF control is shown to be diminished with the use of Butterworth filters to reduce the low-frequency magnitude of the PPF filter. Experimental results show that sound pressure level reductions of the interior full-scale model fairing are maintained above 3.3 dB over the 100- to 250-Hz frequency band as the interior acoustic resonances are changed by more than 5%.

Acknowledgment

The authors would like to thank the U.S. Air Force Research Laboratory for providing funding For this research, under the Small Business Innovation Research (SBIR) program through award number FA9453-04-C-0158.

References

[1] Kemp, J. D., and Clark, R. L., "Noise Reduction in a Launch Vehicle Fairing Using Actively Tuned Loudspeakers," *Journal of the Acoustical Society of America*, Vol. 113, No. 4, 2003, pp. 1986–1994. doi:10.1121/1.1558371

[2] Lane, S. A., Johnson, M., Fuller, C., and Charpentier, A., "Active Control of Payload Fairing Noise," *Journal of Sound and Vibration*, Vol. 290, Nos. 3–5, 2006, pp. 794–819. doi:10.1016/j.jsv.2005.04.017

[3] Estève, S. J., "Control of Sound Transmission into Payload Fairings Using Distributed Vibration Absorbers and Helmholtz Resonators," Ph.D. Dissertation, Virginia Polytechnic Inst. and State Univ., Blacksburg, VA, 2004.

[4] Farinholt, K., "Modal and Impedance Modeling of a Conical Bore for Control Applications," M.S. Thesis, Virginia Polytechnic Inst. and State Univ., Blacksburg, VA, 2001.

[5] Kidner, M. R. F., Fuller, C. R., and Gardner, G., "Increase in Transmission Loss of Single Panels by Addition of Mass Inclusions to a Poro-Elastic Layer: Experimental Investigation," *Journal of Sound and Vibration*, Vol. 294, No. 3, 2006, pp. 466–472. doi:10.1016/j.jsv.2005.11.022

[6] "Minotaur I User's Guide," Release 2.0, Orbital Sciences Corp., Dulles, VA, 2004.

[7] Howard, C. Q., Hansen, C. H., and Zander, A., "Vibro-Acoustic Noise Control Treatments for Payload Bays of Launch Vehicles: Discrete to Fuzzy Solutions," *Applied Acoustics*, Vol. 66, No. 11, 2005, pp. 1235–1261. doi:10.1016/j.apacoust.2005.04.009

[8] Lane, S. A., Griffin, S., and Leo, D., "Active Structural-Acoustic Control of Composite Fairings Using Single-Crystal Piezoelectric Actuators," *Smart Materials and Structures*, Vol. 12, No. 1, 2003, pp. 96–104. doi:10.1088/0964-1726/12/1/311

[9] Hughes, W. O., McNelis, A. M., and Himelblau, H., "Investigation of Acoustic Fields for the Cassini Spacecraft: Reverberant Versus Launch Environments," 5th AIAA/CEAS Aeroacoustics Conference and Exhibit, Bellevue, WA, AIAA Paper 99-1985, Vol. 2, 10–12 May 1999.

[10] Lane, S. A., Clark, R. L., and Southward, S. C., "Active Control of Low Frequency Modes in an Aircraft Fuselage Using Spatially Weighted Arrays," *Journal of Vibration and Acoustics*, Vol. 122, No. 3, 2000, pp. 227–234. doi:10.1115/1.1303848

[11] Sacarcelik, O., "Acoustic Devices for the Active and Passive Control of Sound in a Payload Compartment," M.S. Thesis, Virginia Polytechnic Inst. and State Univ., Blacksburg, VA, 2004.

[12] Creasy, M. A., Leo, D. J., and Farinholt, K. M., "Adaptive Positive Position Feedback for Energy Absorption in Acoustic Cavities," *Journal of Sound and Vibration*, Vol. 311, Nos. 1–2, Mar. 2008, pp. 461–472.. doi:10.1016/j.jsv.2007.09.013

[13] Astrom, K. J., and Wittenmark, B., *Adaptive Control*, 2nd ed., Addison Wesley, Reading, MA, 1995.

[14] Goodwin, G. C., and Sin, K. S., *Adaptive Filtering Prediction and Control*, Prentice–Hall, Englewood Cliffs, NJ, 1984.

[15] Krstic, M., Kanellakopoulos, I., and Kokotovic, P. V., *Nonlinear and Adaptive Control Design*, Wiley, New York, 1995.

[16] Narendra, K. S., and Annaswamy, A. M., *Stable Adaptive Systems*, Prentice–Hall, Englewood Cliffs, NJ, 1980.

[17] Sastry, S., and Bodson, M., *Adaptive Control: Stability, Convergence, and Robustness*, Prentice–Hall Englewood Cliffs, NJ, 1989.

[18] Inman, D. J., *Engineering Vibration*, 2nd ed., Prentice–Hall, Upper Saddle River, NJ, 2001.

[19] Fanson, J. L., and Caughey, T. K., "Positive Position Feedback Control for Large Space Structures," *AIAA Journal*, Vol. 28, No. 4, 1990, pp. 717–724.

[20] McEver, M. A., and Leo, D. J., "Autonomous Vibration Suppression Using On-Line Pole-Zero Identification," *Journal of Vibration and Acoustics*, Vol. 123, No. 4, 2001, pp. 487–495. doi:10.1115/1.1385836

[21] Dorf, R. C., and Bishop, R. H., *Modern Control Systems*, 9th ed., Prentice–Hall, Upper Saddle River, NJ, 2001.

[22] Clark, R. L., Cole, D. G., and Framption, K. D., "Phase Compensation for Feedback Control of Enclosed Sound Fields," *Journal of Sound and Vibration*, Vol. 195, No. 5, 1996, pp. 701–718. doi:10.1006/jsvi.1996.0457

[23] Clark, R. L., and Cole, D. G., "Active Damping of Enclosed Sound Fields through Direct Rate Feedback Control," *Journal of the Acoustical Society of America*, Vol. 97, No. 3, 1995, pp. 1710–1716. doi:10.1121/1.412049

[24] Smith, A. K., and Vipperman, J. S., "Adaptive Resonant Mode Acoustic Controller," 2005 ASME International Mechanical engineering Congress and Exhibit (IMECE2005), Orlando, FL, American Society of Mechanical Engineers Paper IMECE2005-89279, 5–11 Nov. 2005.

L. Peterson
Associate Editor